Article

UDC 681.527.74:539.23(045)

https://doi.org/10.31489/2025PH2/35-46

Received: 25.02.2025

Accepted: 01.04.2025

Zh.Zh. Akhatova[1], B.R. Ilyassov[1]✉, G.S. Seisenbayeva[1],
D.S. Kambar[1], A.K. Aimukhanov[2], L.S. Aldasheva[1], A.V. Zavgorodniy[1]

[1]*Astana IT University, Mangilik El 55/11, Block C1, 010000 Astana, Kazakhstan;*
[2]*Karaganda Buketov University, Karaganda, Kazakhstan*

Electrochemical rectifying device based on polymer thin films

In this work we study the rectifying behavior of organic electrochemical transistors (OECTs). Despite OECT devices are symmetric devices they display asymmetrical output IV curves at negative and positive drain bias sweep. Here, we show that the asymmetry is introduced by the electrical connections with the drain (or source) potential affecting the distribution of ion density in the channel that tunes the doping/de-doping state of the channel and consequently modulates its conductivity. This effect is profoundly noticeable on accumulation mode OECT based on Poly(3-hexylthiophene) (P3HT) channel layer. We demonstrate that accumulation mode OECT can operate either as a current rectifier with the positive rectification polarity or as a current rectifier with the negative rectification polarity by simple changing connection of the gate electrode either directly to the source or to the drain, respectively. The underline mechanism of the current rectification and hystereses in IV curves of OECT based rectifier are discussed. At the forward V_{ds} sweep, the doping of the drain region occurs due to the injection of anions driven by positive ΔV. During the forward scan, the channel begins in a highly conductive state, resulting in higher forward current. In contrast, during the backward scan, the channel is more resistive, leading to lower current. Besides the capacitive hysteresis caused by ion inertia, the intrinsic capacitive hysteresis associated with electronic charging/discharging and polarization due to lateral ion movement also contributes to the observed hysteresis.

Keywords: organic electrochemical transistor, electrochemical transistor rectifier, electrochemical transistor diode, asymmetric IV curve, inductive hysteresis, ionic-electronic conductor, P3HT layer

✉*Corresponding author*: Ilyassov Baurzhan, baurzhan.ilyassov@astanait.edu.kz

Introduction

Electrochemical rectifiers based on organic thin films represent a new class of functional devices that harness the interplay between ionic and electronic transport mechanisms to achieve nonlinear current-voltage (I–V) behavior [1–4]. These devices differ fundamentally from conventional semiconductor diodes, which rely on charge carrier separation at p-n junctions to produce rectification [5]. Instead, electrochemical rectifiers operate through the modulation of the charge carrier density in a semiconducting polymer by ionic species from an electrolyte. This process, known as electrochemical doping and de-doping, provides a unique platform for constructing low-voltage, flexible, and biocompatible electronic components using soft materials [6–10].

The emergence of organic mixed ionic-electronic conductors (OMIECs) has significantly expanded the scope of organic electronics. These materials support simultaneous ionic and electronic conduction [11], enabling new types of devices that bridge the gap between traditional electronics and electrochemical systems. Among OMIECs, poly(3-hexylthiophene) (P3HT) is one of the most widely studied due to its ease of processing, structural tunability, and well-characterized optoelectronic properties [12–14]. While P3HT has been primarily used in organic field-effect transistors (OFETs) [15], photovoltaic cells [16–18], and sensors [19], its electrochemical properties have gained increasing attention, particularly in the context of organic electrochemical transistors (OECTs) [20–22]. In OECTs, the application of a gate voltage causes ion penetration into the polymer bulk, modulating its conductivity via bulk electrochemical doping [23]. This mode of operation makes OECTs highly sensitive to ionic environments, thus ideal for applications in biosensing and neuromorphic computing.

Interestingly, the OECT architecture can be reconfigured into a two-terminal rectifying element by electrically connecting the gate to either the source or drain electrode [4]. In such configurations, the gate potential becomes fixed with respect to one terminal, and the drain potential effectively governs the electrochemical state of the channel. This results in asymmetric doping/de-doping dynamics along the channel length,

leading to I-V characteristics that exhibit diode-like rectification. The rectifying behavior in these organic electrochemical systems is not due to Schottky barriers or built-in potentials, but rather to the spatially non-uniform ionic modulation of conductivity driven by electrochemical gradients. This sets them apart from traditional diodes and brings their operation closer to that of nanofluidic diodes [24], ionic memristors [25], and artificial synapses.

Understanding the rectification mechanisms in these soft electronic devices is essential for unlocking their potential in logic circuits, bioelectronics, and energy conversion. However, despite recent interest, systematic investigations of electrochemical rectification in polymer-based devices remain limited. There is still a lack of clarity on how factors such as device geometry, material morphology, gate connection scheme, and bias polarity influence the degree of rectification. Moreover, the role of ionic dynamics in shaping the time-dependent response of such devices — including hysteresis and inductive effects — is not fully understood. These factors are critical for designing stable and efficient rectifiers that can operate under practical conditions.

In this work, we report the fabrication and in-depth characterization of an electrochemical rectifying device based on an amorphous thin film of P3HT, configured in an OECT-like architecture. Using interdigitated indium tin oxide (ITO) electrodes on glass and a planar electrolyte interface, we construct a geometry that allows us to study the asymmetric modulation of channel conductivity. We demonstrate that when the gate is connected to the source or drain, the device exhibits strong diode-like I-V curves with rectification ratios exceeding an order of magnitude at zero gate bias. This two-terminal configuration simplifies the device operation and opens the door to integration with passive circuit elements. Our recent work [4] presents a comprehensive analytical model that captures the key physical mechanisms governing the operation of organic electrochemical rectifiers, forming the theoretical basis for the present study.

We further investigate the origin of the rectification by combining current-voltage measurements with impedance spectroscopy and cyclic voltammetry, we identify the contributions of ionic motion and charge redistribution to the observed asymmetry and hysteresis in the I-V curves. We also observe the emergence of inductive features in impedance spectra at low frequencies, consistent with previously reported chemical inductance in other mixed-conductor systems such as halide perovskites [26–28]. Our results reveal that the dynamic electrochemical behavior of the channel is highly sensitive to both the direction and rate of voltage sweeps, reflecting the inherent ion-electron coupling and slow ionic response.

The findings presented in this study offer new insights into the operation of electrochemical rectifiers and provide a foundation for the rational design of next-generation devices based on organic semiconductors and electrolytes. By harnessing electrochemical rectification in OMIEC materials, it becomes possible to construct soft, printable diodes and memory elements that operate efficiently in aqueous or physiological environments, paving the way for their application in wearable electronics, implantable devices, and neuromorphic circuits.

Experimental

Organic electrochemical rectifiers with the architecture of OECT is fabricated using P3HT as the active material in the channel. P3HT (LT-S909) was purchased from Luminescence Technology Corp. As source-drain electrodes interdigitated pre-patterned ITO glass substrates from Ossila (S161: Width × Length: 30 mm × 50 μm) were used. P3HT solution was prepared by dissolving 25 mg of polymer in 1 ml chlorobenzene in a glovebox with an inert atmosphere. The solution was stirred during 3 hours at 45 ^{o}C before spin-coating. ITO patterned source-drain substrates were rigorously cleaned. First, substrates were sonicated in DI water with a detergent for 10 mins, and then were rinsed three times by DI water, followed by a sonication in acetone and IPA for 10 mins. Finally, substrates were dried by nitrogen flow and were treated by UV-ozone (UV Ozone Cleaner with UV intensity is approximately 15 mW/cm² at 185 nm, L2002A3-EU, Ossila) for 15 minutes in order to remove any residual organics and improve wettability of the substrate surface.

P3HT channel layers were casted by a spin-coating technique. 30μL of the P3HT solution at 45 °C were dropped on substrate spinning at rate of 1000 rpm and was kept rotating for 1 minute. As-casted P3HT films were further used without annealing in an amorphous state. According to the works of Ginger and his co-workers, amorphous P3HT based OECTs mostly operate in electrochemical mode [20, 21]. 20 mM KCl aqueous solution was used as electrolyte and Ag wire served as a gate electrode. IV curves were measured by a 2 channel Keithley source meter controlled by a customized LabVIEW program. The impedance spectra were probed by PalmSens4 potentiostat with Impedance Analyzer.

Results and Discussion

Rectification behavior of OECT

The simplified diagram of accumulation mode OECTs is depicted in Figure 1*A*. The interdigitated ITO on a glass substrate was used as source and drain electrodes. An amorphous P3HT layer, 20 mM KCl aqueous solution and Ag wire were used as a channel, an electrolyte and a gate, respectively. The P3HT based OECT, which is the accumulation mode device, is on turn off state at the absence of the gait bias (V_{gs} = 0 V). At V_{gs} = 0 V, the P3HT channel has a negligible density of holes and as a result a low conductivity. By applying the negative gate bias relative to the source, the conductivity of the channel can be increased dramatically. Under an appropriate negative V_{gs}, anions (Cl^-) from electrolyte are injected into the bulk of P3HT and consequently equivalent amount of holes will be inserted from the source (at V_{ds} < 0) in order to electronically compensate for charges of anions. This phenomenon is called an electrochemical doping. Biasing the drain relative to the source generates an electric current in the channel (I_{ds}), the value of which depends on the applied V_{gs}. The more negative V_{gs} results in higher I_{ds} at fixed V_{ds} due to the increased channel conductivity resulted from the electrochemical doping. However, the (de)doping of ions is driven not only by the gate bias but in addition it is affected by the drain (or source) potential interfering the electrochemical doping.

The output curves of P3HT OECT are shown in Figure 1*B*. The output curves at various gate biases (V_{gs}) were measured at negative and positive drain bias (V_{ds}) polarities relative to the source in order to reveal inherent rectifying feature of OECT. As can be seen from Figure 1*B*, OECT output curves are asymmetrical, current values at positive V_{ds} sweep is higher in comparison with negative V_{ds} sweep. This asymmetry in the output curve is more profound at V_{gs} = 0 V. The rectification ratios at V_{ds} = ±0.3 V for different gate biases are listed in Table. At V_{gs} = 0 V, OECT shows the highest rectification ratio, the current at forward bias (V_{ds} > 0) at least one order of magnitude larger in comparison with reversed current (V_{ds} < 0). We observe that the more negative gate bias noticeable mitigates this IV asymmetry due to enhanced doping of the channel.

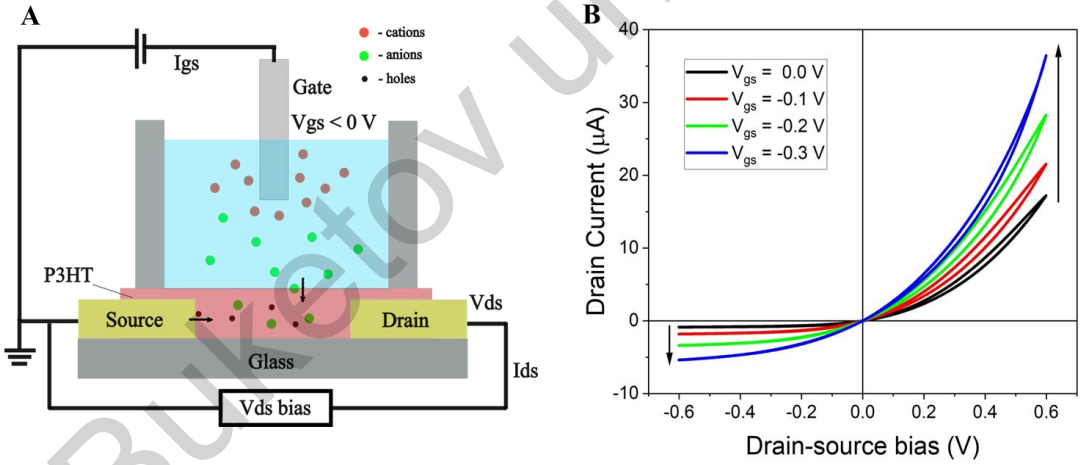

Figure 1. The schematic representation of the P3HT based OECT [4] and its output curves at various gate bias. The output curves were measured at the V_{ds} sweep in both negative and positive values relatives to the source

T a b l e

Rectification ratio of the drain current at different gate biases

Gate bias (V_{gs})/*V*	Current (μA) at V_{ds}: –0.3 V	Current (μA) at V_{ds}: +0.3 V	Rectification ratio
0.0	0.32	4.1	12.8
–0.1	1.6	6.3	3.9
–0.2	2.8	8.4	3.0
–0.3	4.1	10.3	2.5

The rectifying ratio of the OECT is more profound at V_{gs} = 0 V, therefore it is straightforward to use OECT as a current rectifier at V_{gs} = 0 V, which allow simplifying the OECT into a two terminal device. The simplest approach to maintain V_{gs} at 0 V is to connect it directly to the source electrode, which is a common

technique in MOSFET in order to use a transistor as a diode [29]. However it is worth mentioning that typical MOSFET contains a shunting diode, which passes current when the source and drain are shorted and without the shunting diode MOSFET will have symmetric IV curves. The electrical connection of the OECT with the shorted gate and source and its corresponding IV curve is represented in Figure 2. For comparison IV curves of a pristine amorphous P3HT layer (before adding the electrolyte) and the same device without the gate electrode is also shown. The IV characteristics in Figure 2 and in the following Figures were measured in the range of V_{ds} of –0.4 V to +0.6 V. It is due fact that the wider range of V_{ds} caused irreversible change of the channel conductivity.

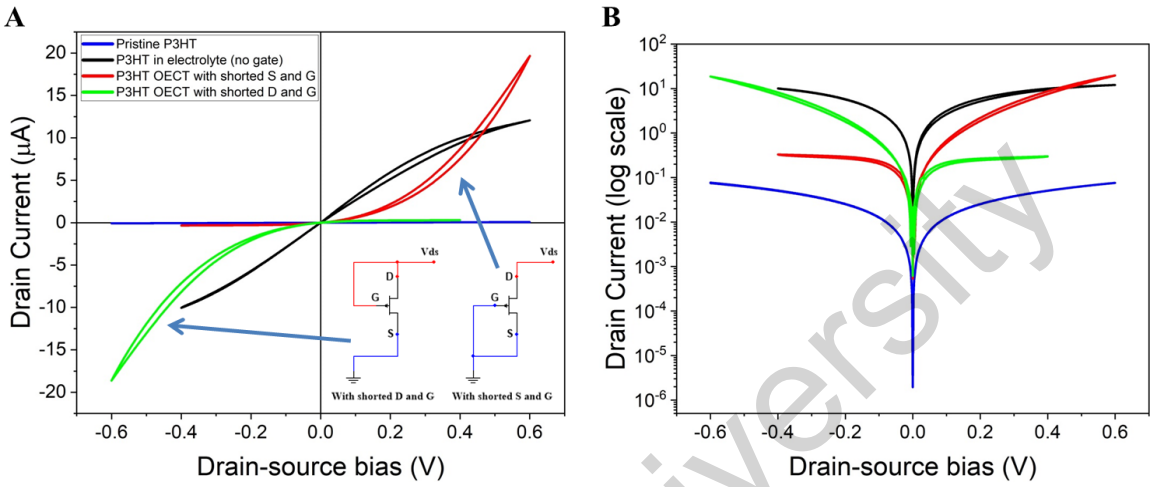

Figure 2. The schematic representation of OECT with shorted gate and source and shorted gate and drain and their IV characteristics
(For comparison IV of pristine P3HT and P3HT in electrolyte without gate are also plotted)

The IV curve of the device without gate is almost symmetrical, which highlights the importance of the gate for the current rectification. Without gate electrode, in a perfectly aligned device (where the channel length is much greater than the overlap between the interfaces of electrolyte/channel/electrode), the IV curve of the device would be symmetric [3]. However, in real devices, this interface overlap area is not negligible, and this contact overlap forms an electrochemical double layer causing the electrochemical electrode coupling (EEC), which can cause asymmetric IV curve in OECT devices without a gate [3]. This EEC phenomenon drives inhomogeneous (de)doping of ions and strongly dependents on device geometry. In the case when the gate is presented, the rate of (de)doping of ions is governed by the potential difference between the gate and the channel, where the potential of the channel along its length is nonuniform [30–32].

As was seen from Figure 2, OECT with shorted gate and source electrodes reveals diode like IV curve. At the positive V_{ds}, the device is more conductive and at the negative V_{ds} it is highly resistive. We associate this phenomenon with the effect of the drain on doping/de-doping of the channel (Fig. 3). At negative V_{ds} sweep, we detect a low current which is comparable with a current in the pristine P3HT implying that the channel is de-doped (Fig. 3*A*). Though, this de-doping is not uniform along the channel length and more profound close to the drain. However, at the positive V_{ds} sweep, the device shows a significantly higher current, which indicate about doping of the channel during the scan (Fig. 3*B*). Similarly, this doping also is not uniform. It is worth mentioning that this highly asymmetrical IV curve of P3HT OECT resembles the IV curve of nanofluidic rectifiers based on nanopores [24, 33]. However, the underline rectifying mechanism is completely different.

One can argue that the enhanced drain current in positive V_{ds} sweep can be the leakage current which can originate between electrolyte/P3HT/drain overlap areas. However, the contribution of the leakage current on I_{ds} can be easily analyzed by comparing I_{ds} with I_g (gate current) due to I_g current is the sum of the channel charging current and the leakage current. Therefore, the origin of this diode-like IV curve of OECT with shorted source and gate is attributed with the effect of the drain potentials on doping/de-doping process.

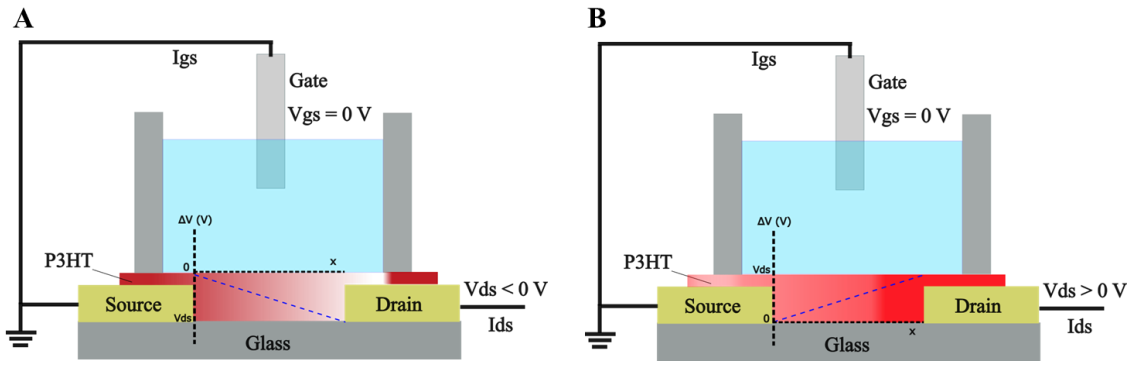

Blue dotted line shows an overly simplified channel potential (ΔV) along its length relative to the gate. The gradient of the channel color is oversimplified doping state of the channel: in the case of Figure 3*A* cherry red colored regions are initial low de-doped state, whereas more bleached regions are de-doped state. Oppositely, in the case of Figure 3*B*, low faintly bleached regions are initial low de-doped state and reddish regions are doped state. The charge carriers are not shown

Figure 3. Simplified diagrams of de-doping (*A*) and doping (*B*) of the channel governed by the drain potential

The potential along the length of the channel (ΔV) is not constant (Fig. 3). It is 0 V near the source and either increases or decreases toward the drain, depending on the polarity of the V_{ds}, up to the value of the drain potential near the drain. The source and gate is shorted and the potential difference ΔV ($V_{ch} - V_g$) between the channel region near the source and the gate is 0 V and always fixed to this value. Therefore there is no any ion driving force perpendicular to the channel near the source region, which governs doping/de-doping process. In contrast, the situation is completely different around the channel region near the drain. The drain region potential is changing during the V_{ds} sweep, which causes the change of the magnitude and the direction of the driving force of the doping/ de-doping process at that region. The ΔV is changing and its sign depends on the V_{ds} polarity.

At the negative V_{ds} sweep, the potential of P3HT region from the drain and toward the source is negative relative to the gate and its value increases, which creates ion driving force pattern pushing absorbed anions back to the solution and pulling cations into the channel, therefore causing de-doping of P3HT. At the more negative V_{ds} the state of the de-doping increases and the volume of this depleted region broadens towards the source, which overall contributes to the decrease of the P3HT film conductivity. In contrast, at the positive drain bias sweep, the region around the drain becomes more conductive due to the increase of the anion density caused by positive ΔV. The sweep of V_{ds} to more positive values will further increase the anion density and widen this enriched region toward the source. As result, the conductivity of the film increases.

As it was shown by the previous discussion, the accumulation mode OECT with shorted gate and source electrodes function as a two terminal rectifier with the positive polarity rectification. However, the rectification polarity can be easily reversed by changing the connection of the gate. In Figure 2, an electrical connection of OECT with shorted gate and drain electrodes and its IV curve is shown as well. As the IV curve indicates, the OECT with shorted gate and drain behaves as a rectifier with negative high current. At the positive V_{ds} sweep the current is low and is comparable to the current of the pristine P3HT device. However, at the negative V_{ds} sweep the current is higher by at least one order.

The IV curve of the OECT with shorted gate and drain is almost mirror reflection of the IV curve of the OECT with shorted gate and source. The rectifying mechanism is identical; however the doping/de-doping processes are governed by the source electrode. During V_{ds} sweep, ΔV near the drain region is 0 V (due to $V_{gs} = V_{ds}$) and fixed, whereas at the source region ΔV is changing due to change of gate potential, which is connected to the drain. At positive V_{ds} sweep, $\Delta V < 0$, the gate is more positive relative the source, which causes an intake of cations and pushing anions out. This causes de-doping of the channel region near the source and widening its volume toward the drain, which leads to the decrease of the channel conductivity and lower current at positive V_{ds} sweep. At negative V_{ds} sweep, near the source $\Delta V > 0$, which creates the pattern of ion driving force pushing anions into the channel and extracting cations. Overall, the density of holes increases leading to the growth of channel conductivity and to enhanced I_{ds}.

Hysteresis in IV curves

Electrochemical devices typically have strong hystereses in cyclic voltammetry IV curves. The origin of the hystereses can be various. In this section we will discuss the hystereses originating from sluggish ion response on a potential perturbation. In OECTs, (de)doping rate is limited by ion mobility in the channel, which is significantly smaller in the comparison with the hole mobility. This ion sluggishness usually reveals itself in cyclic voltammetry as hysteresis in varies electronic devices involving ion migration due to the applied bias [34–37]. Similarly, in IV curves of OECTs, we observe hystereses, when the current measured at forward scan does not coincide with the current probed at the backward scan. The hysteresis in IV curves of OECTs is inherent phenomenon and in the most cases it is caused by slow response of ions to V_{gs} or V_{ds} change [38, 39].

In Figure 4, cyclic IV curves of the OECT rectifier with shorted gate and source at positive V_{ds} sweep measured at various scan rates (V_r) are depicted. Each IV curves at a fixed scan rate was measured at least two times in order to make sure that observed hystereses are kinetic. We should clarify that these IV curves on Figure 4, technically, is output curves of OECT at V_{gs} = 0. However, due to the significant effect of the drain on the channel doping/de-doping process, these IV curves are not measured at the steady-state gate current. During the V_{ds} sweep the gate current changes causing doping and de-doping of the channel. This (de)doping of the channel during the CV measurement causes hystereses.

In cyclic IV curves of the OECT rectifier at positive V_{ds}, we observe inductive hysteresis, which is attributed with the slow response of ions to the change of ΔV. At the forward V_{ds} sweep, the doping of the drain region occurs due to the injection of anions driven by positive ΔV. When the V_{ds} reaches the turning point, the channel has been doped to some extend to a more conductive state and during the backward V_{ds} sweep de-doping takes place, but the channel is in the slightly higher conductive state, which causes the higher backward current and the observed hysteresis. The doping and de-doping of the channel is not fast and is limited by an ion drift diffusion rate.

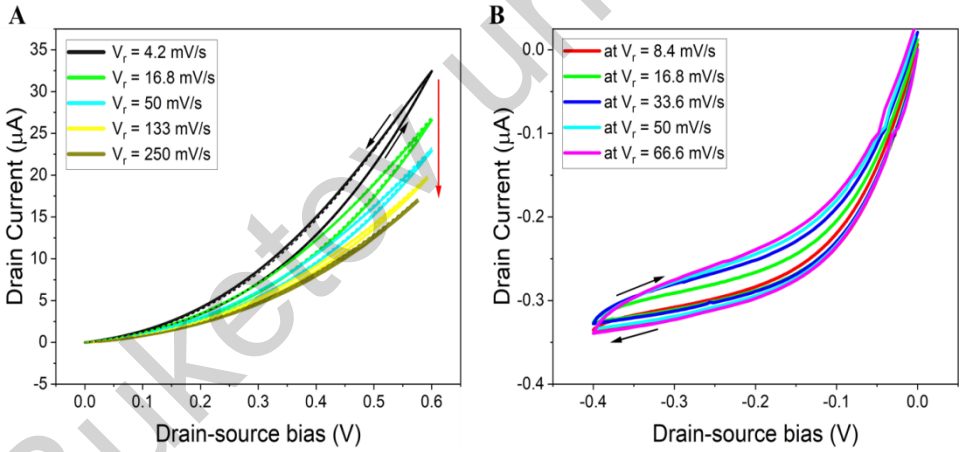

Measurements at each V_r were measured at least two times; second scans were performed after initials with 15 sec delay and they are shown as dotted lines.
For (*B*) seconds scans are shown in Figure 5

Figure 4. Cyclic voltammetry measurements at positive (*A*) and negative (*B*) V_{ds} sweep

The increase of V_{ds} scan rate affects the hysteresis strength and the value of drain current. As can be seen from Figure 4*A* the hysteresis strength shrinks by increasing V_r and the overall current is decreasing (shown in Figure 4 by a red arrow), which can be explained by the ion slow response to ΔV change. At faster V_r, the channel cannot reach the density of anions that it can do at slower V_r due to ions have less time to dope the channel at the same V_{ds} sweep range and therefore it is less conductive at higher V_r. The collapse of the inductive hysteresis at higher V_r, we attribute with capacitive contribution of the channel. V_{ds} also causes lateral ion movements in the channel, which polarizes the channel [31, 40, 41]. As can be seen from Figure 4, the competition of two types of hystereses results in hysteresis-free IV curve in OECT rectifier at higher positive V_{ds} sweep rate.

The cyclic IV curves of OECT with shorted gate and source at negative V_{ds} sweep also have hystereses. However, in contrast to IV curves in the first quadrant (at positive V_{ds}), the hystereses in IV curves in the third quadrant at negative V_{ds} sweep are purely capacitive (Fig. 4*B* and 5). Ion slow response to ΔV change can also cause capacitive hysteresis. It depends what occurs at the forward and backward V_{ds} scan: doping and de-doping or vice versa. If it is doping at the forward scan and de-doping at the backward one, the hysteresis is inductive, what we have discussed earlier. Oppositely, at negative V_{ds} sweep during the forward scan it occurs de-doping of the channel, which is more intense near the drain and widens with the decreased intensity toward to the source. Indeed, at negative V_{ds}, the potential difference ΔV is 0 V near the source and growing negatively toward the drain, which causes intake of cations and extraction of anions resulting in the channel depletion (de-doping). At the backward V_{ds} sweep occurs doping due to ΔV value is decreasing and the channel returns to its more conductive state. During the forward scan, the channel starts in a highly conductive state, resulting in a higher forward current. In contrast, during the backward scan, the channel becomes more resistive, leading to a lower current. In addition to the capacitive hysteresis originated from ion inertia, the inherent capacitive hysteresis related with electronic charging/discharging phenomena and polarizing due to the lateral ion shift can also contribute to the observed hysteresis.

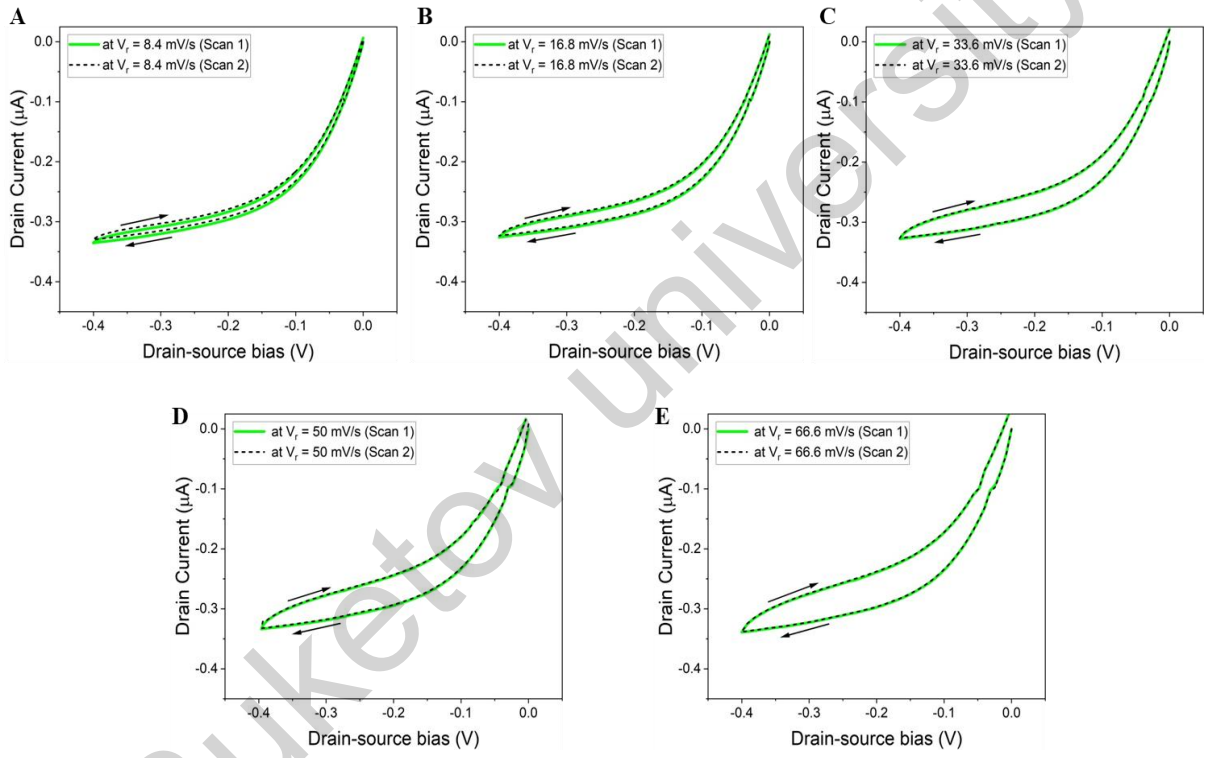

CV curves were measured at V_{ds} scan rates (V_r) 8.4 mV/s to 66 mV/s.
Measurements at each V_r were measured at least two times; second scans were performed after initials with 15 sec delay and they are shown as dotted lines

Figure 5. Cyclic voltammetry measurements at negative V_{ds} sweep

Additionally, as can be seen from Figure 5 more clearly, with the increase of V_r, the strength of the capacitive hysteresis magnifies. It is also seen from Figure 4*B* that at the forward scans the current level for each V_r are approximately identical; however the backward currents at higher V_r are noticeably lower in comparison with the backward currents probed at lower V_r. These both trends indicate that at higher V_r other electronic charging/discharging phenomena more profoundly contribute to the hystereses.

Inductive response in impedance spectra

Inductive hystereses in IV curves also often reported in halide perovskite based devices such as solar cells, photodetectors, LEDs and memristors [34–39]. In many electronic devices, hysteresis is undesired effect due to it complicates the evaluation of device performance and can result to unreliable device operation. Though for some devices such as memristors it is intrinsic property which determines its functionality [42].

As regards OECTs, the usefulness of hysteresis will dependent on its application. Therefore a deeper understanding of hysteresis originated from the slow dynamic motion of ions through the electrolyte/channel interface and in the channel itself is important in order to mitigate it or oppositely enhance its strength and reproducibility for specific application.

Impedance spectroscope technique is one of the useful tools to study charge transfer processes in multilayered electronic devices [26, 36, 43]. In perovskite based devices, observed inductive hystereses are also detected in impedance spectra (IS) in the form of negative loops at low frequencies [27], which obtained the designation as a chemical inductance [28]. However in OECT, which is a three terminal device, the measurement and analysis of IS not straightforward. Though in the case of OECT with shorted gate and source or shorted gate and drain, the device becomes two terminal and the IS spectra between source and drain can be easily measured. The small AC perturbation applied to the drain will affect both electronic current and additionally ionic current, which with some delay will affect the electronic current.

In Figure 6, the measured IS of the P3HT OECT with shorted gate and source electrodes are shown. IS were measured at the various V_{ds} bias from –0.1 V to +0.5 V and at the AC frequency range from 1 MHz to 10 mHz. All measured IS at different V_{ds} compose of three arcs: large arc located in the middle of IS is clearly related with channel resistance and capacitance. We observe that at negative V_{ds}, the middle arc dimeter is too large, whereas at positive V_{ds} its value is decreasing (Fig. 6), which is consistent with the IV curve of the device.

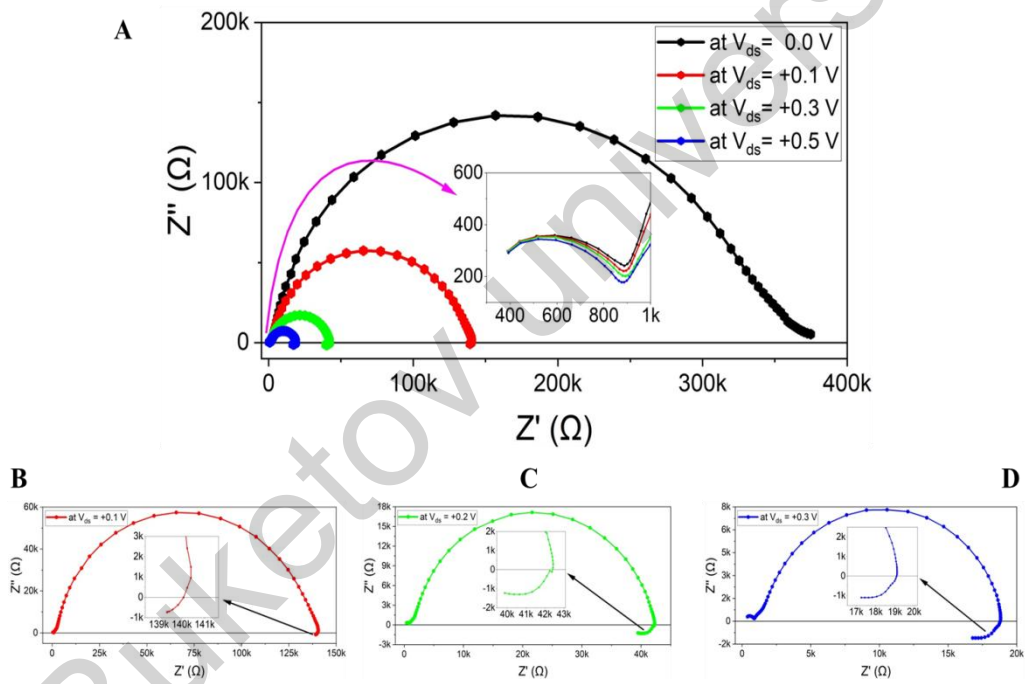

A — Impedance spectra measured at V_{ds} bias from 0 V to + 0.5 V;
B, C, D — IS at V_{ds} = +0.1 V, V_{ds} = +0.3 V, and V_{ds} = +0.5 V, respectively

Figure 6. Impedance spectra of OECT with shorted gate and source

At high frequencies there is a small arc in all IS, which does not depend on V_{ds} (the inset in Figure 6A). In the IS of pristine P3HT device (without electrolyte) this small arc is absent. However, it is present in the device with electrolyte but without gate, which implies that this arc in the high frequency range presumably represents double layer at the electrolyte/P3HT/electrode interface.

The IS responses at low frequencies are significantly different at both V_{ds} polarities. At negative –0.1 V and 0 V it has mixed diffusion and *RC* characteristics, whereas at positive V_{ds}, we observe inductive loops curling in negative Z" toward the origin (Fig. 6*B-D*). This type of negative loops at low frequencies are common in IS of perovskite based devices associate with slow transients in the current upon ion displacement under bias change [44]. In the same manner, small AC perturbation in OECT causes ion displacement (doping/de-doping) and slow transient of the I_{ds}.

In contrast to the perovskite based devices, in OECT ion drift is two dimensional: (perpendicular) across the channel, which is governed by gate-channel potential difference and (lateral) along the channel, which is determined by potential difference between the drain and the source. The robust electrical equivalent circuit is needed in order to properly fit experimental IS and evaluate charge transport characteristics. The detail analysis of IS of OECTs is beyond the scope of this work and will be addressed in future works. Nevertheless, the observed inductive loop in IS at positive V_{ds} is consistent with inductive hysteresis in OECT output curve, which confirm the concept of last studies showing that slow motion of ions in mixed ionic-electronic devices is universal phenomenon related to the hysteresis in the current-voltage characteristics [43]. A recent effort by J. Bisquert proposed an equivalent circuit for OECTs that incorporates the key features of mixed conduction and transient ionic response [44]. However, this model continues to evolve and requires further refinement and validation across different device configurations and operational regimes.

Conclusions

This work has revealed underestimated rectifying functionality of OECTs. OECTs inherently have asymmetrical output curves caused by the effect of the drain potential. Despite this phenomenon is undesired feature in OECT operation, it can be utilized for the development of organic electrochemical rectifiers (diodes) for printable electronics. The same OECT device can be used as polarity switchable rectifier by changing the connection of the gate electrodes. The origin of rectifying behavior of OECT is proposed based on enormous studies in OECT analysis of IV characteristics. The significant asymmetry in IV curve of OECT with shorted gate and source and shorted gate and drain are related with the enormous effect of the drain (or source) potential, which can modulate doping and de-doping state in the channel. However, detail studies are needed to obtain deep understanding of the rectifying characteristics and to derive solid theoretical model of transient current of OECT based rectifiers. Moreover, it is not clear how the device geometry and channel material properties will affect the rectifying characteristics of OECTs, which require more rigorous studies. Nevertheless, this work reminds overlooked rectifying property of OECTs enabling them found a new application in organic electronics, bioelectronics and neuromorphic computing.

Acknowledgments

We thank the Science Committee of the Ministry of Science and Higher Education of the Republic of Kazakhstan for financial support under the project Grant No. AP19576727. B. Ilyassov expresses his sincere gratitude to Prof. Juan Bisquert and Prof. Antonio Guerrero from INAM, Universitat Jaume I, for providing the valuable opportunity to receive research training at INAM sponsored by Bolashak International Scholarship, focusing on the development and characterization of organic electrochemical transistors (OECTs).

References

1 Chen, M., Nilsson, D., Kugler, T., Berggren, M., & Remonen, T. (2002). Electric current rectification by an all-organic electrochemical device. *Applied Physics Letters, 81*(11), 2011–2013. https://doi.org/10.1063/1.1506785

2 Kim, Y., Kim, G., Ding, B., Jeong, D., Lee, I., Park, S., Kim, B.J., McCulloch, I., Heeney, M., & Yoon, M. (2022). High-Current-Density organic electrochemical diodes enabled by asymmetric active layer design. *Advanced Materials, 34*(7). https://doi.org/10.1002/adma.202107355

3 Weissbach, A., Cucchi, M., Tseng, H., Leo, K., & Kleemann, H. (2023). Unraveling the electrochemical electrode coupling in integrated organic electrochemical transistors. *Advanced Functional Materials, 33*(46). https://doi.org/10.1002/adfm.202302205

4 Ilyassov, B., Zavgorodniy, A., Alekseev, A., & Aldasheva, A. (2024b). Rectifying behavior of organic electrochemical transistors. *Physica B Condensed Matter*, 416620. https://doi.org/10.1016/j.physb.2024.416620

5 Sze, S.M., & Ng, K.K. (2006). *Physics of semiconductor Devices*, 293–296. https://doi.org/10.1002/0470068329

6 Organic Electrochemical Transistors as an Emerging Platform for Bio-Sensing Applications: A review. *IEEE Sensors Journal, 21*(4), 3977–4006. https://doi.org/10.1109/jsen.2020.3033283

7 Flexible organic electrochemical transistors for bioelectronics. *Cell Reports Physical Science, 4*(11), 101673. https://doi.org/10.1016/j.xcrp.2023.101673

8 Feron, K., Lim, R., Sherwood, C.P., Keynes, A., Brichta, A.M., & Dastoor, P.C. (2018). Organic Bioelectronics: Materials and biocompatibility. *International Journal of Molecular Sciences, 19*(8), 2382. https://doi.org/10.3390/ijms19082382

9 Ohayon, D., & Inal, S. (2020). Organic bioelectronics: from functional materials to Next-Generation devices and power sources. *Advanced Materials, 32*(36). https://doi.org/10.1002/adma.202001439

10 Torricelli, F., Adrahtas, D.Z., Bao, Z., Berggren, M., Biscarini, F., Bonfiglio, A., Bortolotti, C.A., Frisbie, C.D., Macchia, E., Malliaras, G.G., McCulloch, I., Moser, M., Nguyen, T., Owens, R.M., Salleo, A., Spanu, A., & Torsi, L. (2021). Electrolyte-gated transistors for enhanced performance bioelectronics. *Nature Reviews Methods Primers, 1*(1). https://doi.org/10.1038/s43586-021-00065-8

11 Paulsen, B.D., Fabiano, S., & Rivnay, J. (2021). Mixed Ionic-Electronic transport in polymers. *Annual Review of Materials Research, 51*(1), 73–99. https://doi.org/10.1146/annurev-matsci-080619-101319

12 Kleinschmidt, A.T., Root, S.E., & Lipomi, D.J. (2016). Poly(3-hexylthiophene) (P3HT): fruit fly or outlier in organic solar cell research? *Journal of Materials Chemistry A, 5*(23), 11396–11400. https://doi.org/10.1039/c6ta08317j

13 Ludwigs, S. (2014). P3HT revisited — from molecular scale to solar cell devices. In *Advances in polymer science*, 265, 24–27. https://doi.org/10.1007/978-3-662-45145-8

14 Agbolaghi, S., & Zenoozi, S. (2017). A comprehensive review on poly(3-alkylthiophene)-based crystalline structures, protocols and electronic applications. *Organic Electronics, 51*, 362–403. https://doi.org/10.1016/j.orgel.2017.09.038

15 Runfang, H., Yangfan, Y., Leilei, L., Jianlong, J., Qiang, Z., Lifeng, D., Shengbo, S., & Qiang, L. (2022). P3HT-based organic field effect transistor for low-cost, label-free detection of immunoglobulin G. *Journal of Biotechnology, 359*, 75–81. https://doi.org/10.1016/j.jbiotec.2022.09.022

16 Ghosekar, I.C., & Patil, G.C. (2021). Review on performance analysis of P3HT:PCBM-based bulk heterojunction organic solar cells. *Semiconductor Science and Technology, 36*(4), 045005. https://doi.org/10.1088/1361-6641/abe21b

17 Rozhkova, X.S., Aimukhanov, A.K., Ilyassov, B.R., Tussupbekova, A.K., Zeinidenov, A.K., Alexeev, A.M., Zhakanova, A.M. (2023). Effect of WS_2 nanoparticles on the current-voltage characteristics of a polymer solar cell. *Bulletin of the University of Karaganda – Physics*, (109) 1, 13–22. https://doi.org/10.31489/2023PH1/13-22

18 Omarbekova, G.I., Aimukhanov, A.K., Ilyassov, B.R., Alexeev, A.M., Zeinidenov, A.K., & Zhakanova, A.M. (2023). Effect of the thickness and surface interface of In_2O_3 films on the transport and recombination of charges in a polymer solar cell. *Bulletin of the University of Karaganda – Physics*, (110) 2, 17–24. https://doi.org/10.31489/2023PH2/17-24

19 Cheng, S., Wang, Y., Zhang, R., Wang, H., Sun, C., & Wang, T. (2023). Recent progress in gas sensors based on P3HT Polymer Field-Effect transistors. *Sensors, 23*(19), 8309. https://doi.org/10.3390/s23198309

20 Giridharagopal, R., Flagg, L.Q., Harrison, J.S., Ziffer, M.E., Onorato, J.W., Luscombe, C.K., & Ginger, D.S. (2017b). Electrochemical strain microscopy probes morphology-induced variations in ion uptake and performance in organic electrochemical transistors. *Nature Materials, 16*(7), 737–742. https://doi.org/10.1038/nmat4918

21 Flagg, L.Q., Giridharagopal, R., Guo, J., & Ginger, D.S. (2018). Anion-Dependent doping and charge transport in organic electrochemical transistors. *Chemistry of Materials, 30*(15), 5380–5389. https://doi.org/10.1021/acs.chemmater.8b02220

22 Colucci, R., De Paula Barbosa, H.F., Günther, F., Cavassin, P., & Faria, G.C. (2019). Recent advances in modeling organic electrochemical transistors. *Flexible and Printed Electronics, 5*(1), 013001. https://doi.org/10.1088/2058-8585/ab601b

23 Rivnay J., Inal S., Salleo A., Owens R. M., Berggren M., & Malliaras G. G. (2018). Organic electrochemical transistors. *Nature Reviews Materials, 3*(2). https://doi.org/10.1038/natrevmats.2017.86

24 Ramirez, P., Portillo, S., Cervera, J., Bisquert, J., & Mafe, S. (2024). Memristive arrangements of nanofluidic pores. *Phys. Review E. 109*(4), 044803. https://doi.org/10.1103/PhysRevE.109.044803

25 Xu, G., Zhang, M., Mei, T., Liu, W., Wang, L., & Xiao, K. (2024). Nanofluidic ionic memristors. *ACS Nano*. https://doi.org/10.1021/acsnano.4c06467

26 Bou, A., & Bisquert, J. (2021). Impedance spectroscopy dynamics of biological neural elements: from memristors to neurons and synapses. *The Journal of Physical Chemistry B, 125*(35), 9934–9949. https://doi.org/10.1021/acs.jpcb.1c03905

27 Ebadi, F., Taghavinia, N., Mohammadpour, R., Hagfeldt, A., & Tress, W. (2019). Origin of apparent light-enhanced and negative capacitance in perovskite solar cells. *Nature Communications, 10*(1). https://doi.org/10.1038/s41467-019-09079-z

28 Bisquert, J., & Guerrero, A. (2022). Chemical inductor. *Journal of the American Chemical Society, 144*(13), 5996–6009. https://doi.org/10.1021/jacs.2c00777

29 Emadi, A., Khaligh, A., Nie, Z., & Lee, Y.J. (2017). Integrated power electronic converters and digital control. In *CRC Press eBooks*. https://doi.org/10.1201/9781439800706

30 Robinson, N.D., Svensson, P., Nilsson, D., & Berggren, M. (2006b). On the Current Saturation Observed in Electrochemical Polymer Transistors. *Journal of the Electrochemical Society, 153*(3), H39. https://doi.org/10.1149/1.2172534

31 Kaphle, V., Paudel, P.R., Dahal, D., Krishnan, R.K.R., & Lüssem, B. (2020). Finding the equilibrium of organic electrochemical transistors. *Nature Communications, 11*(1). https://doi.org/10.1038/s41467-020-16252-2

32 Skowrons, M., Dahal, D., Paudel, P.R., & Lüssem, B. (2023). Depletion type organic electrochemical transistors and the gradual channel approximation. *Advanced Functional Materials, 34*(4), 2303324. https://doi.org/10.1002/adfm.202303324

33 RamíRez, P., Gómez, V., Cervera, J., Mafé, S., & Bisquert, J. (2023). Synaptical tunability of multipore nanofluidic memristors. *The Journal of Physical Chemistry Letters, 14*(49), 10930–10934. https://doi.org/10.1021/acs.jpclett.3c02796

34 Muñoz-Díaz, L., Rosa, A. J., Bou, A., Sánchez, R.S., Romero, B., John, R.A., Kovalenko, M.V., Guerrero, A., & Bisquert, J. (2022). Inductive and capacitive hysteresis of halide perovskite solar cells and memristors under illumination. *Frontiers in Energy Research, 10*. https://doi.org/10.3389/fenrg.2022.914115

35 Bisquert, J., Guerrero, A., & Gonzales, K.C. (2021). Theory of hysteresis in halide perovskites by integration of the equivalent circuit. *ACS Physical Chemistry Au, 1*(1), 25–44. https://doi.org/10.1021/acsphyschemau.1c00009

36 Bisquert, J. (2024). Inductive and capacitive hysteresis of Current-Voltage curves: unified structural dynamics in solar energy devices, memristors, ionic transistors, and bioelectronics. *PRX Energy, 3*(1). https://doi.org/10.1103/prxenergy.3.011001

37 Bisquert, J., Gonzales, K.C., & Guerrero, A. (2023). Transient On/Off photocurrent response of halide perovskite photodetectors. *The Journal of Physical Chemistry C, 127*(43), 21338–21350. https://doi.org/10.1021/acs.jpcc.3c04672

38 Shameem, R., Bongartz, L.M., Weissbach, A., Kleemann, H., & Leo, K. (2023). Hysteresis in organic electrochemical transistors: relation to the electrochemical properties of the semiconductor. *Applied Sciences, 13*(9), 5754. https://doi.org/10.3390/app13095754

39 Bisquert, J. (2023). Hysteresis in organic electrochemical transistors: Distinction of capacitive and inductive effects. *The Journal of Physical Chemistry Letters, 14*(49), 10951–10958. https://doi.org/10.1021/acs.jpclett.3c03062

40 Paudel, P.R., Kaphle, V., Dahal, D., Krishnan, R.K.R., & Lüssem, B. (2020). Tuning the transconductance of organic electrochemical transistors. *Advanced Functional Materials, 31*(3). https://doi.org/10.1002/adfm.202004939

41 Paudel, P.R., Skowrons, M., Dahal, D., Krishnan, R.K R., & Lüssem, B. (2022). The transient response of organic electrochemical transistors. *Advanced Theory and Simulations, 5*(5). https://doi.org/10.1002/adts.202100563

42 Bisquert, J. (2023a). Current-controlled memristors: Resistive switching systems with negative capacitance and inverted hysteresis. *Physical Review Applied, 20*(4). https://doi.org/10.1103/physrevapplied.20.044022

43 Guerrero, A., Bisquert, J., & Garcia-Belmonte, G. (2021). Impedance Spectroscopy of Metal Halide Perovskite Solar Cells from the Perspective of Equivalent Circuits. *Chemical Reviews, 121*(23), 14430–14484. https://doi.org/10.1021/acs.chemrev.1c00214

44 Bisquert, J. & Keene, S.T. (2024). Using the transversal admittance to understand organic electrochemical transistors. *Advanced Science, 12*, 2410393, 1–24. https://doi.org/10.1002/advs.202410393

Ж.Ж. Ахатова, Б.Р. Ильясов, Г.С. Сейсенбаева, Д.С. Қамбар,
А.К. Аймуханов, Л.С. Алдашева, А.В. Завгородний

Полимерлі жұқа қабықшаларға негізделген электрхимиялық түзеткіш құрылғы

Мақалада органикалық электрхимиялық транзисторлардың (OECTs) түзету сипаттамалары зерттелді. OECT құрылғылары симметриялы құрылғылар болғанына қарамастан, олар ағынның теріс және оң ығысуымен шығыс кернеуінің асимметриялық қисықтарын көрсетеді. Мұнда біз ассимметрияның арнадағы иондар тығыздығының таралуына әсер ететін ағын (немесе көз) потенциалы электрлік қосылыстардан туындайтынын көрсетеміз, бұл арнаның легирлеу/легирлеуді шешу күйін реттейді және осылайша оның өткізгіштігін модуляциялайды. Бұл әсер әсіресе поли(3-гексилтиофен) (P3HT) арна қабатына негізделген OECT жинақтау режимінде байқалады. Жинақтау режиміндегі OECT оң түзету полярлығы бар ток түзеткіш ретінде немесе басқару электродын тікелей көзге немесе ағынға қосып жай ғана өзгерту арқылы теріс түзету полярлығы бар ток түзеткіш ретінде де жұмыс істей алатынын көрсетілген. OECT негізіндегі түзеткіштің IV қисықтарындағы токты түзетудің негізгі механизмі және гистерезис талқыланды. OECT түзеткішінің IV циклдік қисықтарында оң V_{ds} кезінде индуктивті гистерезисті байқаймыз, бұл иондардың ΔV өзгеруіне баяу реакциясымен түсіндіріледі. Тікелей V_{ds} қосылуы кезінде ағынды аймақтың легирленуі оң ΔV туындаған анионды инжекциялау арқылы жүреді. Тікелей сканерлеу кезінде канал жоғары өткізгіштікпен жұмыс істей бастайды, бұл тікелей токтың жоғарылауына әкеледі. Керісінше, кері сканерлеу кезінде канал үлкен кедергіге ие, бұл токтың төмендеуіне әкеледі. Иондық инерциядан туындаған сыйымдылықты гистерезистен басқа байқалатын гистерезис сонымен қатар электронды құрылғыларды зарядтауға/разрядтауға және иондардың бүйірлік қозғалысының поляризациясына байланысты.

Кілт сөздер: органикалық электрхимиялық транзистор, электрхимиялық транзисторлық түзеткіш, электрхимиялық транзисторлық диод, асимметриялық IV қисық, индуктивті гистерезис, иондық-электронды өткізгіш, P3HT қабаты

Ж.Ж. Ахатова, Б.Р. Ильясов, Г.С. Сейсенбаева, Д.С. Қамбар,
А.К. Аймуханов, Л.С. Алдашева, А.В. Завгородний

Электрохимическое выпрямительное устройство на основе тонких полимерных пленок

В статье изучены характеристики выпрямления органических электрохимических транзисторов (OECTs). Несмотря на то, что устройства OECTs являются симметричными, они демонстрируют асимметричные кривые выходного напряжения при отрицательном и положительном смещении стока. Нами показано, что асимметрия возникает из-за электрических соединений с потенциалом стока (или источника), влияющих на распределение плотности ионов в канале, что настраивает состояние легирования/снятия легирования с канала и, следовательно, модулирует его проводимость. Этот эффект особенно заметен в режиме накопления в OECT на основе канального слоя из поли(3-гексилтиофена)

(P3HT). Мы демонстрируем, что OECT в режиме накопления может работать либо как выпрямитель тока с положительной полярностью выпрямления, либо как выпрямитель тока с отрицательной полярностью выпрямления путем простого изменения подключения управляющего электрода либо непосредственно к источнику, либо к стоку, соответственно. Обсуждается основной механизм выпрямления тока и гистерезисы в IV кривых выпрямителя на основе OECT. При прямом сканировании канал начинает работать с высокой проводимостью, что приводит к увеличению прямого тока. Напротив, при обратном сканировании канал обладает большим сопротивлением, что приводит к снижению тока. Помимо емкостного гистерезиса, вызванного инерцией ионов, наблюдаемый гистерезис также обусловлен собственным емкостным гистерезисом, связанным с зарядкой/разрядкой электронных устройств и поляризацией из-за бокового перемещения ионов.

Ключевые слова: органический электрохимический транзистор, электрохимический транзисторный выпрямитель, электрохимический транзисторный диод, асимметричная кривая IV, индуктивный гистерезис, ионно-электронный проводник, слой P3HT

Information about the authors

Akhatova, Zhannur — Researcher, Astana IT University, Astana, Kazakhstan; e-mail: Zh.Akhatova@astanait.onmicrosoft.com; ORCID ID: https://orcid.org/0000-0003-4363-1307

Ilyassov, Baurzhan (*corresponding author*) — PhD, Associate professor, Astana IT University, Astana, Kazakhstan; e-mail: baurzhan.ilyassov@astanait.edu.kz; ORCID ID: https://orcid.org/0000-0003-4563-2004

Seisenbayeva, Gulsaya — Researcher, Astana IT University, Astana, Kazakhstan; e-mail: g.seisenbayeva@astanait.onmicrosoft.com; ORCID ID: https://orcid.org/0009-0003-7004-4498

Kambar, Dinara — Researcher, Astana IT University, Astana, Kazakhstan; e-mail: Kambards97@gmail.com; ORCID ID: https://orcid.org/0000-0003-4742-2000

Aimukhanov, Aitbek — Professor, Karaganda Buketov University, Karaganda, Kazakhstan; e-mail: aitbekaimukhan@gmail.com; ORCID ID: https://orcid.org/0000-0002-4384-5164

Aldasheva, Laura — PhD, Associate professor, Astana IT University, Astana, Kazakhstan; e-mail: Laura.Aldasheva@astanait.edu.kz; ORCID ID: https://orcid.org/0000-0001-6815-1989

Zavgorodniy, Alexey — PhD, Astana IT University, Astana, Kazakhstan; e-mail: a.zavgorodniy@astanait.onmicrosoft.com; ORCID ID: https://orcid.org/0000-0002-3024-7237